Review Article

The value of ^{18}F-fluorodeoxyglucose positron emission tomography-based radiomics in non-small cell lung cancer

Yu-Hung Chen[a,b,c], Kun-Han Lue[a], Sung-Chao Chu[c,d]*, Chih-Bin Lin[e], Shu-Hsin Liu[a,b]

[a]Department of Medical Imaging and Radiological Sciences, Tzu Chi University, Hualien, Taiwan, [b]Department of Nuclear Medicine, Hualien Tzu Chi Hospital, Buddhist Tzu Chi Medical Foundation, Hualien, Taiwan, [c]School of Medicine, College of Medicine, Tzu Chi University, Hualien, Taiwan, [d]Department of Hematology and Oncology, Hualien Tzu Chi Hospital, Buddhist Tzu Chi Medical Foundation, Hualien, Taiwan, [e]Department of Internal Medicine, Hualien Tzu Chi Hospital, Buddhist Tzu Chi Medical Foundation, Hualien, Taiwan

Abstract

Currently, the second most commonly diagnosed cancer in the world is lung cancer, and 85% of cases are non-small cell lung cancer (NSCLC). With growing knowledge of oncogene drivers and cancer immunology, several novel therapeutics have emerged to improve the prognostic outcomes of NSCLC. However, treatment outcomes remain diverse, and an accurate tool to achieve precision medicine is an unmet need. Radiomics, a method of extracting medical imaging features, is promising for precision medicine. Among all radiomic tools, ^{18}F-fluorodeoxyglucose positron emission tomography (^{18}F-FDG PET)-based radiomics provides distinct information on glycolytic activity and heterogeneity. In this review, we collected relevant literature from PubMed and summarized the various applications of ^{18}F-FDG PET-derived radiomics in improving the detection of metastasis, subtyping histopathologies, characterizing driver mutations, assessing treatment response, and evaluating survival outcomes of NSCLC. Furthermore, we reviewed the values of ^{18}F-FDG PET-based deep learning. Finally, several challenges and caveats exist in the implementation of ^{18}F-FDG PET-based radiomics for NSCLC. Implementing ^{18}F-FDG PET-based radiomics in clinical practice is necessary to ensure reproducibility. Moreover, basic studies elucidating the underlying biological significance of ^{18}F-FDG PET-based radiomics are lacking. Current inadequacies hamper immediate clinical adoption; however, radiomic studies are progressively addressing these issues. ^{18}F-FDG PET-based radiomics remains an invaluable and indispensable aspect of precision medicine for NSCLC.

Keywords: *[18]F-fluorodeoxyglucose positron emission tomography, Deep learning, Heterogeneity, Non-small cell lung cancer, Radiomics*

Introduction

Lung cancer ranks the second in global cancer statistics and is responsible for the most cancer-related deaths around the world [1,2]. Approximately 127,070 lung cancer-related deaths have been reported in the United States in 2023 [2]. Lung cancers are classified into small cell and non-small cell lung cancer (NSCLC). In all lung cancer cases, NSCLC accounts for approximately 85%, and primarily adenocarcinoma subtype [3]. Early-stage NSCLC can receive curative-intended treatment and achieve favorable survival outcomes; however, most NSCLC cases present as metastatic disease on diagnosis owing to a lack of initial symptoms, resulting in poor prognosis [1,3-5]. Over recent decades, understanding oncogenic drivers and immunology has led to the emergence of targeted treatments and immune checkpoint inhibitors (ICIs), improving the prognosis of NSCLC [3,6,7]. However, about half of the patients experience disease progression within 1 year despite initial response, with even higher rates for ICI recipients [3,7-10]. Furthermore, these novel therapies are not without toxicities [11,12]. Precision tools are crucial for selecting patients who may benefit from these novel treatments when minimizing adverse effects, and research in achieving precision medicine is growing.

To date, ^{18}F-fluorodeoxyglucose positron emission tomography (^{18}F-FDG PET) has been clinically applied for pretreatment staging, therapeutic response assessment, and detecting recurrence of NSCLC [3]. It serves as a biomarker of enhanced glycolysis, reflecting the metabolic reprogramming of cancer and providing prognostic values [13-15]. Therefore, ^{18}F-FDG PET is ideal for

*Address for correspondence: Dr. Sung-Chao Chu, Department of Hematology and Oncology, Hualien Tzu Chi Hospital, Buddhist Tzu Chi Medical Foundation, 707 Section 3, Chung-Yang Road, Hualien, Taiwan. E-mail: oldguy-chu1129@umail.hinet.net

How to cite this article: Chen YH, Lue KH, Chu SC, Lin CB, Liu SH. The value of ^{18}F-fluorodeoxyglucose positron emission tomography-based radiomics in non-small cell lung cancer. Tzu Chi Med J 2025;37(1):17-27.

stratifying the risk of NSCLC and enabling risk-adapted precision medicine. In routine clinical practice, the interpretation of ^{18}F-FDG PET is usually qualitative; however, quantitative imaging features extracted from ^{18}F-FDG PET, known as ^{18}F-FDG PET-based radiomics, are now extensively utilized as research biomarkers for NSCLC. The number of scientific articles on ^{18}F-FDG PET-based radiomics in NSCLC exceeds a hundred on PubMed, suggesting the popularity of this research topic.

This review concisely introduces ^{18}F-FDG PET-based radiomics and summarizes the current research categories in NSCLC. We then emphasize the possible pathophysiological basics, pitfalls, and future directions of using ^{18}F-FDG PET-based radiomics in NSCLC. Finally, ^{18}F-FDG PET-based deep learning (DL) with convolutional neural network (CNN) for NSCLC is briefly reviewed.

RADIOMICS BASED ON ^{18}F-FLUORODEOXYGLUCOSE POSITRON EMISSION TOMOGRAPHY

Radiomics involves extracting and analyzing numerous quantitative features from medical images, enabling the description and quantification of subtle traits on the images beyond what is visually perceptible. We can extract radiomic features from anatomical images, such as computed tomography (CT) or magnetic resonance imaging (MRI), as well as molecular images, such as ^{18}F-FDG PET. As the underlying molecular process of ^{18}F-FDG PET is glycolysis, ^{18}F-FDG PET-based radiomics provides distinct information compared to anatomical imaging-based radiomics [16].

Figure 1 summarizes the imaging processing and radiomic feature extraction from ^{18}F-FDG PET images. The voxel values of ^{18}F-FDG PET are usually normalized according to body weight and injected radioactivity, resulting in a standardized uptake value (SUV), which represents the basic glycolytic intensity. Some institutions also use lean body mass for normalization. Metabolic tumor volume (MTV) and total lesion glycolysis (MTV multiplied SUV_{mean}) are volumetric features, which are commonly used in clinical practice and research entities to describe glycolytic volume. In addition, SUV histograms (first-order voxel statistics) and texture analyses synthesize more complex imaging features. The texture analysis converts images into matrices to extract relevant features. Commonly used matrices in the literature include the gray-level co-occurrence matrix (GLCM) [17], gray-level run length matrix (GLRLM) [18], gray-level size zone matrix (GLSZM) [19], neighborhood gray-level dependence matrix [20], and neighborhood gray-tone difference matrix (NGTDM) [13,21]. The SUV histogram-derived features and texture features are able to describe the
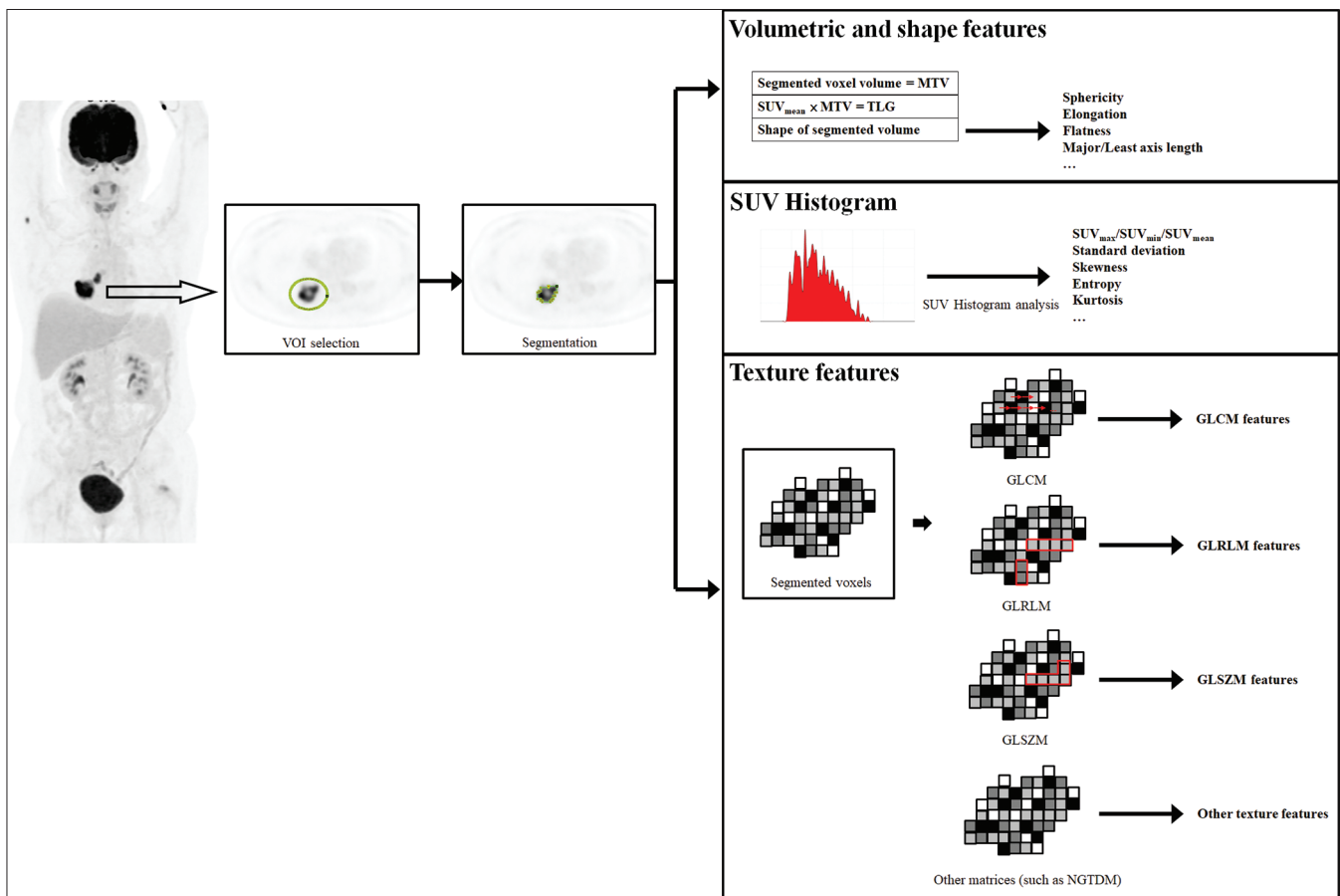
Figure 1: Schematic diagram of ^{18}F-fluorodeoxyglucose positron emission tomography-based radiomic analysis. ^{18}F-FDG PET: ^{18}F-fluorodeoxyglucose positron emission tomography, VOI: Volume-of-interest, SUV: Standardized uptake value, MTV: Metabolic tumor volume, TLG: Total lesion glycolysis, GLCM: Gray-level co-occurrence matrix, GLRLM: Gray-level run length matrix, GLSZM: Gray-level size zone matrix, NGTDM: Neighboring gray-tone difference matrix

glycolytic heterogeneity of ^{18}F-FDG PET [22,23]. Moreover, wavelet decomposition, characterized by its multiresolution spatial-frequency analysis, can be implemented in texture analysis [24]. Finally, shape features can be used to describe the geometric properties of the target lesion. Therefore, ^{18}F-FDG PET-based radiomics can provide information on the geometric characteristics, glycolytic intensity, volume, and heterogeneity of the selected lesion.

Radiomic features are numerous, especially when including wavelet-transformed features, which can result in hundreds of features to describe a lesion. Conventionally, the feature definitions and naming have been inconsistent among studies. Thus, adhering to the imaging biomarker standardization initiative (IBSI) guidelines for radiomic feature extraction and analysis is recommended to avoid inconsistency in the radiomic feature definition [25]. Several software platforms, such as LIFEx and PyRadiomics, follow the IBSI definitions and are available for radiomic analyses [26,27]. Using IBSI-defined analytical methods is required to avoid inconsistencies and promote data generalizability.

THE USE OF ^{18}F-FLUORODEOXYGLUCOSE POSITRON EMISSION TOMOGRAPHY-BASED RADIOMICS IN NON-SMALL CELL LUNG CANCER

The applications of ^{18}F-FDG PET-based radiomics in NSCLC can be classified into several categories [Table 1]. We conducted a comprehensive PubMed search to collect relevant literature on this topic. The terms or keywords for searching materials for different clinical applications included radiomics, FDG PET, fluorodeoxyglucose, positron emission tomography, NSCLC, lung cancer, adenocarcinoma, texture, epidermal growth factor receptor (EGFR), anaplastic lymphoma kinase (ALK), ROS1, pathology, metastasis, survival, and outcomes. The references for each application are listed in Table 1.

SUBTYPING HISTOPATHOLOGIES

^{18}F-FDG PET-based radiomics can be applied in discriminating between histopathologies of NSCLC [Table 2]. Kang *et al.* integrated ^{18}F-FDG PET/CT-derived radiomics with manual diagnosis to differentiate benign inflammatory processes from primary lung malignancy. This combination reduced the false-positive rate from 30.6% to 5.4% and 9.1% in the training and validation cohorts, respectively [28]. In addition, ^{18}F-FDG PET/CT-derived radiomic features have been used to distinguish between primary and metastatic lung diseases [29]. Although less clinically useful, radiomics was also able to subtype the histopathologies of NSCLC [29-31]. Furthermore, Chen *et al.* identified an association between ^{18}F-FDG PET-based heterogeneity feature with higher tumor grades and the invasive histopathological characteristics in lung adenocarcinoma, including lymphovascular and visceral pleural invasion [32]. Finally, an ^{18}F-FDG PET-based radiomic model was reported to distinguish intermediate-to-high risk from lepidic histopathology in early invasive adenocarcinoma [33].

Table 1: The applications of ^{18}F-fluorodeoxyglucose positron emission tomography-based radiomics

Aspects	Applications
Discriminating histopathology	Differentiate benign and malignant disease [28]
	Distinguish primary from metastatic disease [29]
	Histopathological subtyping [29-31]
	Evaluating aggressiveness or invasiveness [32,33]
Predicting metastasis	Improve prediction of lymph node metastasis [23,34-37]
	Improve prediction of brain metastasis [38]
Predicting genetic subtype	Predicting actionable EGFR mutation [39-44]
	Subtyping actionable EGFR mutation [42,44,45]
	Predicting other driver mutations and immune environment [39,43,46-50]
Predicting treatment response and prognosis	Assessing response to treatment and survival outcomes [9,13,22,32,51-60]

^{18}F-FDG PET: ^{18}F-fluorodeoxyglucose positron emission tomography, EGFR: epidermal growth factor receptor

Table 2: The applications of ^{18}F-fluorodeoxyglucose positron emission tomography-based radiomics in discriminating histopathology

Applications	Study	Summary of results
Differentiate between benign and malignant disease	Kang *et al.* [28]	SEN/SPE/FPR/FNR/AUC (training): 91.1%/94.6%/5.4%/8.9%/0.98
		SEN/SPE/FPR/FNR/AUC (validation): 84.6%/90.9%/9.1%/15.4%/0.92
Distinguish primary from metastatic disease	Kirienko *et al.* [29]	SEN/SPE/ACC/AUC (training): 91.6%/66.4%/85.9%/0.92
		SEN/SPE/ACC/AUC (validation): 88.8%/58.4%/82.1%/0.91
Histopathological subtyping	Kirienko *et al.* [29]	SEN/SPE/ACC/AUC to differentiate adenocarcinoma from others (training): 86.0%/74.9%/80.0%/0.90
		SEN/SPE/ACC/AUC to differentiate adenocarcinoma from others (validation): 78.9%/67.9%/72.7%/0.80
	Hyun *et al.* [30]	ACC/AUC: 0.769/0.859
	Han *et al.* [31]	SEN/SPE/ACC/AUC: 0.918/0.809/0.841/0.744
Evaluating aggressiveness or invasiveness	Chen *et al.* [32]	Entropy is associated with tumor grade, lymphovascular invasion, and visceral pleural invasion ($p<0.05$)
	Shao *et al.* [33]	SEN/SPE/ACC/AUC to differentiate lepidic from acinar-papillary group: 0.693/0.833/0.720/0.804

^{18}F-FDG PET: ^{18}F-fluorodeoxyglucose positron emission tomography, SEN: Sensitivity, SPE: Specificity, FPR: False-positive rate, FNR: False-negative rate, ACC: Accuracy, AUC: Area under the receiver operating characteristic curve

IMPROVE PREDICTION OF METASTASIS

One application of radiomics is to improve the prediction of metastases that are less easily detected by visual interpretation [Table 3]. The sensitivity of ^{18}F-FDG PET for the detection of lymph node metastasis of NSCLC is suboptimal, especially for lung adenocarcinoma [61]. False positivity owing to lymphadenitis further complicates visual interpretation [62]. Lue *et al*. discovered that SUV histogram entropy of the primary tumor is an independent predictor of regional nodal metastasis of lung adenocarcinoma. Adding SUV histogram entropy to visual interpretation improved the positive predictive value from 51.2% to 63.0% and the negative predictive value from 75.3% to 82.6% [23]. Other groups have used statistical or machine learning algorithms to combine multiple features into models to maximize the performance of ^{18}F-FDG PET-based radiomics in the prediction of regional nodal metastasis. The reported areas under the receiver operating characteristic curves (AUC) ranged between 0.82 and 0.97 [34-37]. The detection of intracranial metastases is another limitation of ^{18}F-FDG PET owing to its high physiologic activity of the brain [62]. Zheng *et al*. constructed models combining ^{18}F-FDG PET/CT-derived radiomic features, clinical, and pathological characteristics to predict brain metastasis. The c-indices in the training, internal validation, and external validation cohorts were 0.927, 0.861, and 0.860, respectively [38].

PREDICTION OF DRIVER MUTATION OR IMMUNE ENVIRONMENT

The applications of radiomics in predicting NSCLC-related driver mutations and immune microenvironment are outlined in Table 4. Identifying actionable driver mutations is essential in treating NSCLC [3,7]. Approximately half of Asian NSCLC patients present with actionable EGFR mutations and are candidates for targeted therapies [7]. An early retrospective study discovered a lower ^{18}F-FDG SUV_{max} in EGFR-mutant tumors. When combining clinical factors, the model predicted the EGFR mutation status with the AUC of 0.697 [39]. Other studies have developed models with more pretreatment ^{18}F-FDG PET-based radiomics and have demonstrated higher predictive performance (AUC can exceed 0.8) [40-42]. Similar predictive performance has also been demonstrated in studies using machine learning models containing ^{18}F-FDG PET-based radiomic features to classify EGFR mutations [41,43,44]. As different EGFR mutations may exhibit variable survival outcomes [63], ^{18}F-FDG PET-based radiomic models are further used for subtyping between the L858R missense mutation and exon 19 deletion, which are the two most common EGFR mutations [42,44,45]. In addition to EGFR mutations, other rare driver mutations can be targeted [7]. Tumors with ALK or ROS proto-oncogene 1 (ROS1) rearrangement exhibit a higher ^{18}F-FDG avidity [39,46]. However, the radiomic models for predicting ALK or ROS1 rearrangements are less effective than those for predicting EGFR mutations, with AUCs not exceeding 0.700 [39,43,46]. ICIs are one of many therapeutic strategies for NSCLC. The programmed cell death 1 ligand (PD-L1) expression level is associated with the effectiveness of ICI treatment [3]. Many studies have constructed models, including ^{18}F-FDG PET-based radiomics, in predicting positive PD-L1 expression (>1% or >50%) and have demonstrated moderate-to-good performance (AUCs between 0.700 and 0.900) [47-50].

EVALUATION OF PROGNOSTIC OUTCOMES

^{18}F-FDG PET can reflect the viability of tumor, and enhanced glycolysis is related to signaling pathways of malignancies [64,65]. Therefore, ^{18}F-FDG PET is valuable for assessing the response of treatment and prognostic stratification [Table 5]. Dissaux *et al*. reported a model combining two pretreatment ^{18}F-FDG PET-derived radiomic features to predict 2-year local control in patients with early-stage NSCLC receiving stereotactic body radiotherapy. Their model achieved a sensitivity and specificity of 100% and 88%, respectively, in predicting 2-year local control, and the performance was reproduced in the testing set [51]. ^{18}F-FDG PET-derived radiomic features also independently predicted survival outcomes such as disease-free survival (DFS) and progression-free survival (PFS) following radiotherapy [52,53]. Valentinuzzi *et al*. tested the prognostic value of ^{18}F-FDG PET-based radiomics in ICI-treated patients. Radiomics distinguished responders

Table 3: The applications of ^{18}F-fluorodeoxyglucose positron emission tomography-based radiomics in predicting metastasis

Applications	Study	Summary of results
Predicting regional nodal metastasis	Lue *et al*. [23]	Primary tumor entropy-based model. AUC: 0.711
	Laros *et al*. [34]	SEN/SPE/ACC (validation): 85%/0.95%/92%
		SEN/SPE/ACC (testing): 80%/90%/88%
	Qiao *et al*. [35]	SEN/SPE/ACC/AUC (training): 76.3%/89.0%/84.3%/0.884
		SEN/SPE/ACC/AUC (validation): 65.4%/88.4%/79.7%/0.881
	Huang *et al*. [36]	SEN/SPE/ACC/AUC (training): 85.7%/80.4%/82.8%/0.869
		SEN/SPE/ACC/AUC (validation): 64.3%/79.4%/72.6%/0.847
Predicting metastasis in hypermetabolic regional lymph nodes	Ren *et al*. [37][a]	SEN/SPE/FPR/FNR/ACC/AUC (training): 81.7%/87.2%/12.8%/18.3%/84.1%/0.90
		SEN/SPE/FPR/FNR/ACC/AUC (validation): 74.5%/93.6%/6.45%/25.5%/82.1%/0.89
Predicting brain metastasis	Zheng *et al*. [38]	SEN/SPE/AUC (training): 92.3%/85.9%0.91
		SEN/SPE/AUC (validation): 100%/72.7%/0.83

[a]This study enrolled 260 patients with lung cancer, including 249 patients with non-small cell lung cancer and 11 patients with small cell lung cancer.
SEN: Sensitivity, SPE: Specificity, FPR: False-positive rate, FNR: False-negative rate, ACC: Accuracy, AUC: Area under the receiver operating characteristic curve

from nonresponders, and the radiomic model predicted the overall survival (OS) >14.9 months with an AUC of 0.90 [54]. Recently, neoadjuvant immunochemotherapy has been increasingly used in NSCLC to improve the pathological complete response (pCR) rate, with patients with pCR achieving better survival outcomes [66]. Yang *et al.* developed an ^{18}F-FDG PET/CT radiomic model to predict pCR after neoadjuvant immunochemotherapy, showing an AUC of 0.818, which was better than that of the SUV_{max} or CT-based model alone [55], suggesting the potential utility of ^{18}F-FDG PET/CT radiomic model in guiding neoadjuvant immunochemotherapy.

Table 4: The applications of ^{18}F-fluorodeoxyglucose positron emission tomography-based radiomics in predicting genetic mutations and immune environment

Applications	Study	Summary of results
Predicting actionable EGFR mutation	Lv *et al.* [39]	AUC: 0.697
	Zhang *et al.* [40]	SEN/SPE/ACC/AUC (training): 84.54%/74.36%/80.00%/0.86
		SEN/SPE/ACC/AUC (validation): 91.67%/70.27%/80.82%/0.87
	Yang *et al.* [42]	SEN/SPE/ACC/AUC (training): 0.80/0.61/0.71/0.71
		SEN/SPE/ACC/AUC (validation): 0.81/0.57/0.71/0.71
	Agüloğlu *et al.* [43]	ACC/AUC: 71.4%/0.751
	Yang *et al.* [44]	AUC (training): 0.881
		AUC (validation): 0.926
Subtyping EGFR mutation into exon 19 deletion and L858R missense mutation	Yang *et al.* [42]	SEN/SPE/ACC/AUC (training): 0.67/0.85/0.76/0.82
		SEN/SPE/ACC/AUC (validation): 0.88/0.58/0.70/0.73
	Yang *et al.* [44]	AUC (training and validation) to distinguish exon 21 mutation: 0.851 and 0.805
		AUC (training and validation) to distinguish exon 19 mutation: 0.849 and 0.859
	Liu *et al.* [45]	AUC: 0.77 and 0.92 for distinguish exon 19 deletion and L858R missense mutation
Predicting other driver mutations	Lv *et al.* [39]	Higher nodal SUV_{max} in ALK-positive tumors
	Agüloğlu *et al.* [43]	ACC/AUC: 77.4%/0.682 for predicting ALK fusion
	Ruan *et al.* [46]	AUC: 0.873 for predicting ALK fusion
		AUC: 0.813 for predicting ROS1 fusion
Predicting immune microenvironment	Zhou *et al.* [47]	SEN/SPE/AUC (training) to distinguish tumor immune microenvironment: 72.2%/86.7%/0.838
		SEN/SPE/AUC (validation) to distinguish tumor immune microenvironment: 85.7%/76.0%/0.811
	Zhao *et al.* [48]	SEN/SPE/ACC/AUC (training) to predict PD-L1 ≥1%: 61.1%/68.8%/65.2%/0.718
		SEN/SPE/ACC/AUC (validation) to predict PD-L1 ≥1%: 68.5%/68.1%/68.3%/0.769
	Li *et al.* [50]	AUC (predicting PD-L1 over 1%): 0.762
		AUC (predicting PD-L1 over 50%): 0.814

^{18}F-FDG PET: ^{18}F-fluorodeoxyglucose positron emission tomography, EGFR: Epidermal growth factor receptor, ALK: Anaplastic lymphoma kinase, ROS1: ROS proto-oncogene 1, PD-L1: Programmed cell death 1 ligand, SUV_{max}: Maximum standardized uptake value, SEN: Sensitivity, SPE: Specificity, FPR: False-positive rate, FNR: False-negative rate, ACC: Accuracy, AUC: Area under the receiver operating characteristic curve

Table 5: The applications of ^{18}F-fluorodeoxyglucose positron emission tomography-based radiomics in predicting treatment response and prognosis

Applications	Study	Summary of results
Predicting survival in advanced EGFR-mutated lung adenocarcinoma	Lue *et al.* [9]	c-indices of 0.687 for PFS and 0.721 for OS
	Chen *et al.* [22]	c-indices of 0.649 for PFS and 0.691 for OS
Predicting survival in resectable lung adenocarcinoma	Chen *et al.* [32]	c-indices of 0.694 for DFS and 0.704 for OS
Predicting recurrence in early-stage NSCLC treated with SBRT	Dissaux *et al.* [51]	SEN/SPE/ACC/AUC (training): 100%/88%/94%/0.942
		SEN/SPE/AUC (validation): 100%/81%/91%/0.905
Predicting survival in NSCLC treated by SBRT	Lovinfosse *et al.* [52]	Dissimilarity feature was significantly associated with DSS (HR=0.822, *P*=0.037) and with DFS (HR=0.834, *P*<0.01)
Predicting local control in NSCLC treated with SBRT	Takeda *et al.* [53]	High-intensity large-area emphasis was a significant predictor (AUC=0.72)
Predicting response in NSCLC treated with pembrolizumab	Valentinuzzi *et al.* [54]	ACC/AUC: 78%/0.90
Predicting pathological complete response after neoadjuvant immunochemotherapy	Yang *et al.* [55]	AUC: 0.818
Predicting recurrence in resected NSCLC	Ahn *et al.* [57]	ACC/AUC: 90%/0.956
Predicting survival in NSCLC with locoregional disease	Chen *et al.* [58]	c-indices of 0.638 for PFS and 0.725 for OS
Predicting survival in stage III NSCLC undergoing neoadjuvant chemoradiotherapy and surgery	Yoo *et al.* [59]	Radiomics score independently predicted OS (HR=2.297, *P*<0.001)
Predicting survival in lung adenocarcinoma	Zuo *et al.* [60]	c-index of 0.863 for OS

EGFR: Epidermal growth factor receptor, PFS: Progression-free survival, OS: Overall survival, DFS: Disease-free survival, DSS: Disease-specific survival, NSCLC: Non-small cell lung cancer, SBRT: Stereotactic body radiotherapy, SEN: Sensitivity, SPE: Specificity, ACC: Accuracy, AUC: Area under the receiver operating characteristic curve, HR: Hazard ratio

Survival stratification remains one of the most studied applications of ^{18}F-FDG PET-based radiomics in NSCLC [13,67]. ^{18}F-FDG PET-based radiomics has been reported to predict survival outcomes in patients with NSCLC with early disease [32,56,57], locoregional involvement [58,59], and metastatic disease undergoing targeted therapies [9,22,60]. Ahn *et al.* retrospectively studied 93 patients with stage I-III NSCLC and discovered that ^{18}F-FDG PET-derived texture features independently predicted DFS. This PET-derived texture feature remained predictive in a subgroup of patients with stage I-II diseases [57]. Chen *et al.* developed ^{18}F-FDG PET entropy-based models to predict DFS (c-index = 0.694) and OS (c-index = 0.704) in patients with lung adenocarcinoma who underwent curative surgery. Their models outperformed the traditional staging system, histopathological grades, and predominant subtypes and were able to stratify survival outcomes in subgroups based on tumor grades [32]. Their group conducted another retrospective study to test the prognostic value of their models with combined tumor-nodal entropy in nodal-positive NSCLC. Their models predicted PFS (c-index = 0.638) and OS (c-index = 0.725) better than traditional staging systems, and outperformed models with entropy in the primary tumor or lymph nodes alone. Their model performed well in subgroups based on sex, histopathology, and treatment strategies [58]. Yoo *et al.* devised a model based on ^{18}F-FDG PET/CT imaging (the LASSO score), that independently predicted OS in patients with stage III NSCLC underwent neoadjuvant concurrent chemoradiotherapy and surgery. Their LASSO scores demonstrated better performance than conventional PET features [59]. Finally, the survival prognosis of patients with metastatic NSCLC who received EGFR-targeted tyrosine kinase inhibitors (TKI) varied widely [68]. Chen *et al.* and Lue *et al.* employed ^{18}F-FDG PET entropy-based models to predict the PFS (c-index = 0.687) and OS (c-index = 0.721) of patients with EGFR-mutated lung adenocarcinoma following TKI treatment, and their models demonstrated significantly better performance than cancer staging [9,22]. Other groups have constructed complex models, including multiple ^{18}F-FDG PET/CT radiomic features to predict the EGFR mutation status, and their model showed a prognostic value for OS (c-index = 0.863) [60].

CONVOLUTIONAL NEURAL NETWORK-BASED DEEP LEARNING ON ^{18}F-FLUORODEOXYGLUCOSE POSITRON EMISSION TOMOGRAPHY

The aforementioned studies on ^{18}F-FDG PET-based radiomics directly tested the association of clinical data with image features (handcrafted radiomic studies) or used conventional machine learning of image features to formulate prediction models. Another strategy is to utilize a DL CNN to directly analyze and learn the link between ^{18}F-FDG PET and clinical data. For example, Xiao *et al.* trained an EfficientNet-V2 model on ^{18}F-FDG EPT/CT to predict actionable EGFR mutation in NSCLC. The accuracies of their model reached 86.25% in the training cohort and 81.92% in the validation dataset [69]. To predict

metastases, Tau *et al.* used DenseNet to learn ^{18}F-FDG PET images from 264 NSCLC patients. The accuracies of their model for predicting nodal positivity and distant metastasis were 0.80 and 0.63, respectively [70]. In addition, the study by Lue *et al.* investigated the performance of ResNet-50 in predicting the pathological nodal status in lung adenocarcinoma across different PET machines. They reported cross-scanner accuracies of 94.7% and 88.2% in analog and digital PET cohorts, respectively, suggesting that the feasibility of applying DL model across different generations of PET scanners [71]. Data on the capability of DL in predicting survival prognosis are also available. Afshar *et al.* reported c-indices of 0.68 and 0.64 in the prediction of OS and DFS in patients with lung cancers, respectively, using PET/CT-based DL models [72]. Furthermore, Lue *et al.* constructed a model combining DL predictor with clinical variables, ^{18}F-FDG PET-derived avidity feature, and MTV to predict the prognosis of lung adenocarcinoma with actionable EGFR mutation undergoing targeted therapies. The DL-based model can predict the PFS (c-index = 0.738) and OS (c-index = 0.708). The prognostic values were reproduced in the validation cohort using different PET scanners (c-indices of 0.662 and 0.664 for prediction of PFS and OS, respectively) [73].

Studies regarding the applications of ^{18}F-FDG PET-based DL in NSCLC are less abundant than those on handcrafted radiomics or conventional machine learning [41,74]. Nevertheless, the scarce data suggest that DL may outperform traditional radiomic strategies [71,72,74]. For example, in the study by Lue *et al.*, the DL demonstrated better AUCs than radiomics in both analog (AUC of 0.929 vs. 0.676) and digital (AUC of 0.871 vs. 0.697) PET cohorts [71].

CHALLENGES AND FUTURE DIRECTIONS

^{18}F-FDG PET-derived radiomics has been extensively tested for various applications in NSCLC. The application of ^{18}F-FDG PET-derived radiomics is mainly based on the link between glycolytic heterogeneity and clinical outcomes [Figures 2 and 3]. However, many obstacles need to be overcome before implementing in clinical practice. The prerequisite for radiomic research is the availability of extensive and high-quality imaging data. Unlike CT or MRI, which are more popular and more commonly performed in clinical practice, ^{18}F-FDG PET is much less accessible. Ethical issues and data security should also be considered when sharing image data between institutions. Thus, the study materials are less abundant when conducting ^{18}F-FDG PET-based radiomic research. In addition, the radiomic feature extraction from sizable datasets is labor-intensive and time-consuming. Lesion delineation, labeling, volume-of-interest placement, and target segmentation require experienced specialists familiar with the studied imaging modality and disease field. These reasons limit large-scale radiomic studies for ^{18}F-FDG PET.

Another critical issue in translational biomarker research is reproducibility. To generalize radiomic research results and further clinical implementation, investigators must ensure the reliability and robustness of the image features. Radiomic features are susceptible to many factors. For
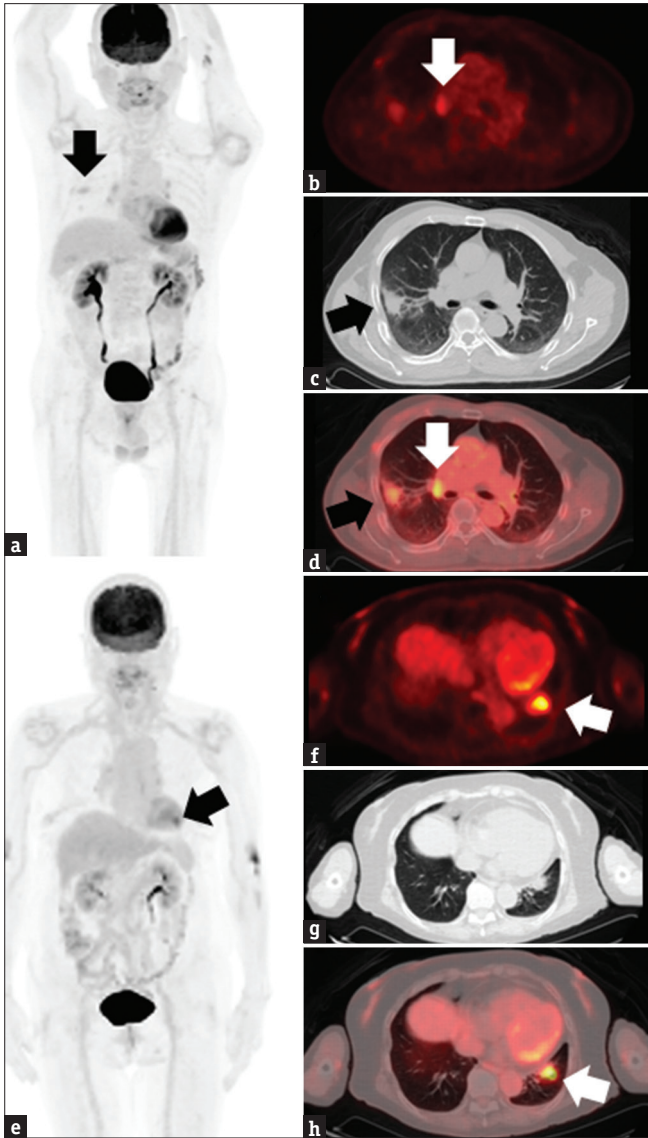
Figure 2: The ^{18}F-fluorodeoxyglucose positron emission tomography (^{18}F-FDG PET/CT) and maximum intensity projection (MIP) images for a 75-year-old man with a primary lung adenocarcinoma in the right lung (a, c, and d, black arrow) with suspicion of ^{18}F-FDG avid right pulmonary hilar node metastasis (b and d, white arrows). The entropy of the primary tumor was 2.6. After curative surgery, the surgical pathology showed no metastasis in the regional lymph nodes. The ^{18}F-FDG PET/CT and MIP images from another 79-year-old woman showed a primary lung adenocarcinoma in the left lower lobe (e-h, arrow). No apparent ^{18}F-FDG avid focus indicating regional nodal metastasis was found. However, the entropy of the primary tumor was 3.9, much higher than the first case, which indicated a higher glycolytic heterogeneity. After curative surgery, the metastatic cells in the peribronchial and subaortic nodes were found. ^{18}F-FDG PET: ^{18}F-fluorodeoxyglucose positron emission tomography, MIP: Maximum intensity projection

Figure 3: The ^{18}F-fluorodeoxyglucose positron emission tomography maximum intensity projection image from a 46-year-old woman with stage IV epidermal growth factor receptor (EGFR)-mutated (L858R missense mutation) lung adenocarcinoma (a). The clinical staging was cT4N3M1c, and the entropy of the primary tumor was 3.0. Another 53-year-old woman with stage IV EGFR-mutated (exon 19 deletion) lung adenocarcinoma (b). The clinical staging was cT2bN3M1b, and the primary tumor entropy was 4.8. Both patients received afatinib treatment. The first patient with a lower entropy experienced disease progression after 20 months. However, the disease control of the later patient, who had a higher tumor glycolytic heterogeneity, lasted for only 11 months. ^{18}F-FDG PET: ^{18}F-fluorodeoxyglucose positron emission tomography, MIP: Maximum intensity projection, EGFR: Epidermal growth factor receptor

example, different scanner parameters, image acquisition settings, reconstruction, and segmentation methods can lead to radiomic feature instability [21]. Many of the early ^{18}F-FDG PET radiomic study results were not replicated across studies [13], possibly because of the different methodologies of the imaging procedures mentioned above. Radiomic features are susceptible at various extents to the affecting factors; therefore, selecting more reproducible features for analysis is essential. Most first-order and shape features are
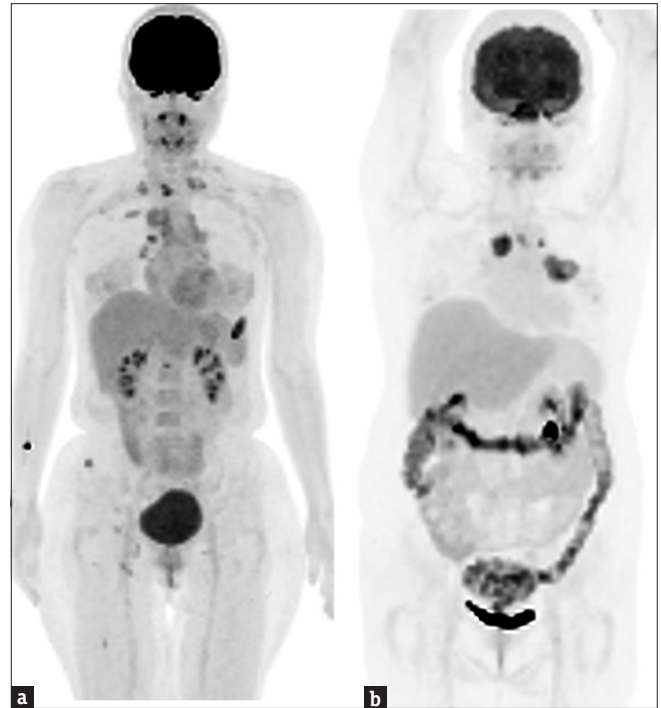
most likely considered robust and reproducible. In contrast, NGTDM-derived features and many GLSZM features are the most sensitive to image processing details [75-79]. The features derived from the remaining texture matrices (such as the GLCM and GLRLM) exhibit widely varied robustness. For example, the GLCM-derived sum entropy shows excellent robustness, whereas the robustness of the GLCM-derived contrast appears to be low [76,78]. Respiratory motion is another critical concern when applying ^{18}F-FDG PET-based radiomics to lung cancer. PET usually requires several minutes for image acquisition at each bed position; thus, respiratory motion obscures the acquired images and may cause partial volume averaging. Selecting radiomic features insensitive to respiratory motion is essential for assessing lesions in the lung. However, most PET-based radiomic features are sensitive to respiratory motion. According to data from different groups, only 3.72%–26.2% of PET features were identified as highly stable [80-82]. Only a few features have been consistently reported to be highly robust to respiratory motion, including sphericity (shape feature), first-order entropy, GLCM-derived sum entropy, and GLRLM-derived run entropy. In contrast, none of the NGTDM features have been consistently reported to be respiratory-stable [80-82]. Notably, most respiratory-stable features are robust against image processing parameters, and

respiratory-sensitive features are generally more susceptible to image processing parameters [75-77,79,81,82].

The underlying biological meanings and explainability of radiomics have been increasingly discussed [21,83]. ^{18}F-FDG PET-based radiomics has been considered a surrogate marker of tumor heterogeneity; however, the notion (that higher clonal heterogeneity may show higher phenotypical heterogeneity) remains hypothetical. Recently, Chen *et al.* prospectively correlated ^{18}F-FDG PET-based radiomic features with whole-exome sequencing results from 46 patients with NSCLC. The first-order entropy positively correlated with genomic heterogeneity (r = 0.31–0.32, P = 0.030–0.036), although the correlation was weak [79]. The weak correlation may be because the glycolytic pathway is only one of the many phenotypes from the genomic expression, and gene expression levels cannot be assessed solely with mutation tests. In addition, the gene sequencing specimen was sampled from the tumor, unlike the whole tumor featuring using PET imaging. Nevertheless, their results provided scientific support for using ^{18}F-FDG PET-based radiomics as a heterogeneity biomarker. The biological meaning of ^{18}F-FDG PET-based radiomics may need basic studies focusing more on the glycolytic pathways to elucidate, for example, comparing ^{18}F-FDG PET-based radiomics with the expression of glucose transporters or hexokinase in the pathological specimens or investigating the correlation between ^{18}F-FDG PET-based radiomics with mutation or expression of genes in the glycolytic pathways. In contrast to radiomics, the biological significance of DL has yet to be scientifically verified. The occlusion method can demonstrate which image parts activate the DL model prediction [Figure 4] [71,84]; however, the underlying mechanism and pathophysiology remain elusive. Furthermore, DL also needs to address reproducibility issues. Novel digital PET scanners exhibit characteristics that differ from those of traditional analog PET scanners [85,86].
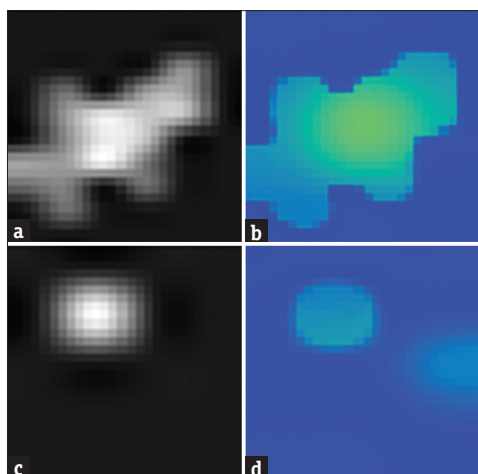

Figure 4: Examples of using activation maps produced by occlusion method for explainability of deep learning model. The upper row shows the tumor image (a) and activation map (b) for positive prediction, while the lower row shows the tumor image (c) and activation map (d) for negative prediction. Note that the activation map shows the valuable areas that indicates positive prediction are located within the tumor

Reports have demonstrated better visual interpretation performance on digital PET scanners than on analog PET scanners; however, DL models trained using analog PET may require procedures, such as transfer learning or filter harmonization, to retain their performance on digital PET scanners [71,73,87].

The prognosis of NSCLC relies on interrogating the disease from different perspectives [Figure 5]. Including radiomics derived from ^{18}F-FDG PET may enable more precise and tailored treatment strategies. However, improving data transparency, protocol standardization, and selecting robust features for analysis are required to enhance the reproducibility and generalizability of ^{18}F-FDG PET-based radiomic models. Furthermore, basic studies linking ^{18}F-FDG PET-based radiomics to genotypes, gene expression profiles, and other phenotypes, such as anatomical images and histopathology, are required to deepen our knowledge of the disease pathophysiology and the underlying mechanisms of radiomics.

CONCLUSIONS

Radiomics is a method to extract quantitative parameters from medical images. ^{18}F-FDG PET-based radiomics provides a way to feature the activity and heterogeneity of glycolysis. To date, ^{18}F-FDG PET-based radiomics has demonstrated its value in various applications of NSCLC, including improving the detection of metastasis, subtyping histopathologies, and characterizing driver mutations. As tumor glycolysis is related to tumor viability and oncogene pathways, ^{18}F-FDG PET-based radiomics is most commonly applied for treatment response and prognostic evaluation. DL is another strategy to maximize the performance of ^{18}F-FDG PET in NSCLC applications. However, several challenges remain unaddressed. ^{18}F-FDG PET-based radiomic studies should ensure reproducibility before being adopted in clinical practice. Basic studies are required to improve our understanding of the underlying biological significance of ^{18}F-FDG PET-based radiomics. Current challenges hinder immediate implementation; nevertheless, radiomic studies are progressively addressing these issues, and ^{18}F-FDG PET-based radiomics remains an invaluable and indispensable aspect of precision medicine for NSCLC.

Declaration of patient consent

The authors certify that they have obtained all appropriate patient consent forms. In the form, the patients have given their consent for their images and other clinical information to be reported in the journal. The patients understand that their names and initials will not be published and due efforts will be made to conceal identity, but anonymity cannot be guaranteed.

Data availability statement

Data sharing is not applicable to this article as no datasets were generated or analyzed during the current study.
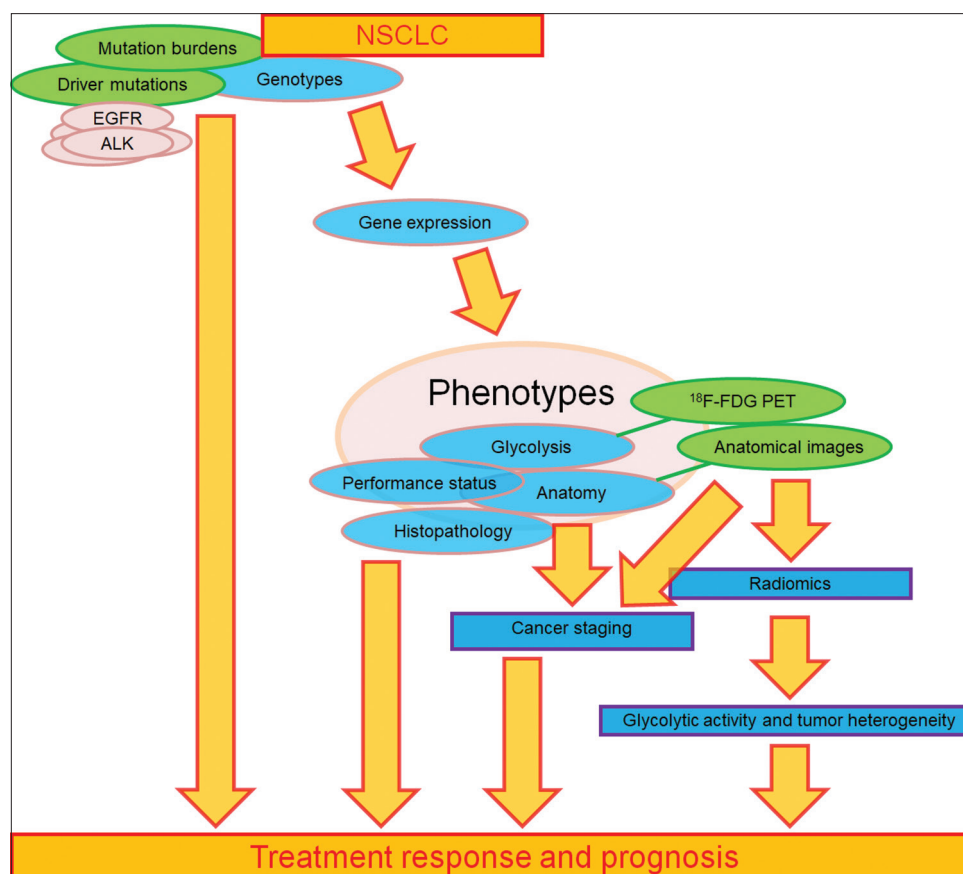
Figure 5: The genotypes and different phenotypes are closely associated with the treatment response and prognosis of non-small cell lung cancer (NSCLC). There are many driver mutations for NSCLC, but we only list the most common ones. NSCLC: Non-small cell lung cancer, ^{18}F-FDG PET: ^{18}F-fluorodeoxyglucose positron emission tomography, EGFR: Epidermal growth factor receptor, ALK: Anaplastic lymphoma kinase

References

1. Sung H, Ferlay J, Siegel RL, Laversanne M, Soerjomataram I, Jemal A, et al. Global cancer statistics 2020: GLOBOCAN estimates of incidence and mortality worldwide for 36 cancers in 185 countries. CA Cancer J Clin 2021;71:209-49.

2. Siegel RL, Miller KD, Wagle NS, Jemal A. Cancer statistics, 2023. CA Cancer J Clin 2023;73:17-48.

3. Thai AA, Solomon BJ, Sequist LV, Gainor JF, Heist RS. Lung cancer. Lancet 2021;398:535-54.

4. Detterbeck FC, Chansky K, Groome P, Bolejack V, Crowley J, Shemanski L, et al. The IASLC lung cancer staging project: Methodology and validation used in the development of proposals for revision of the stage classification of NSCLC in the forthcoming (eighth) edition of the TNM classification of lung cancer. J Thorac Oncol 2016;11:1433-46.

5. Goldstraw P, Chansky K, Crowley J, Rami-Porta R, Asamura H, Eberhardt WE, et al. The IASLC lung cancer staging project: Proposals for revision of the TNM stage groupings in the forthcoming (eighth) edition of the TNM classification for lung cancer. J Thorac Oncol 2016;11:39-51.

6. Mamdani H, Matosevic S, Khalid AB, Durm G, Jalal SI. Immunotherapy in lung cancer: Current landscape and future directions. Front Immunol 2022;13:823618.

7. Tan AC, Tan DS. Targeted therapies for lung cancer patients with oncogenic driver molecular alterations. J Clin Oncol 2022;40:611-25.

8. Mok TS, Wu YL, Kudaba I, Kowalski DM, Cho BC, Turna HZ, et al. Pembrolizumab versus chemotherapy for previously untreated, PD-L1-expressing, locally advanced or metastatic non-small-cell lung cancer (KEYNOTE-042): A randomised, open-label, controlled, phase 3 trial. Lancet 2019;393:1819-30.

9. Lue KH, Huang CH, Hsieh TC, Liu SH, Wu YF, Chen YH. Systemic inflammation index and tumor glycolytic heterogeneity help risk stratify patients with advanced epidermal growth factor receptor-mutated lung adenocarcinoma treated with tyrosine kinase inhibitor therapy. Cancers (Basel) 2022;14:309.

10. Niemeijer AN, Oprea-Lager DE, Huisman MC, Hoekstra OS, Boellaard R, de Wit-van der Veen BJ, et al. Study of (89)Zr-pembrolizumab PET/CT in patients with advanced-stage non-small cell lung cancer. J Nucl Med 2022;63:362-7.

11. Mekki A, Dercle L, Lichtenstein P, Marabelle A, Michot JM, Lambotte O, et al. Detection of immune-related adverse events by medical imaging in patients treated with anti-programmed cell death 1. Eur J Cancer 2018;96:91-104.

12. Shyam Sunder S, Sharma UC, Pokharel S. Adverse effects of tyrosine kinase inhibitors in cancer therapy: Pathophysiology, mechanisms and clinical management. Signal Transduct Target Ther 2023;8:262.

13. Han S, Woo S, Suh CH, Kim YJ, Oh JS, Lee JJ. A systematic review of the prognostic value of texture analysis in (18)F-FDG PET in lung cancer. Ann Nucl Med 2018;32:602-10.

14. Chen YH, Chu SC, Wang LY, Wang TF, Lue KH, Lin CB, et al. Prognostic

value of combing primary tumor and nodal glycolytic-volumetric parameters of (18)F-FDG PET in patients with non-small cell lung cancer and regional lymph node metastasis. Diagnostics (Basel) 2021;11:1065.

15. Kim G, Kim J, Cha H, Park WY, Ahn JS, Ahn MJ, et al. Metabolic radiogenomics in lung cancer: Associations between FDG PET image features and oncogenic signaling pathway alterations. Sci Rep 2020;10:13231.

16. Torigian DA, Huang SS, Houseni M, Alavi A. Functional imaging of cancer with emphasis on molecular techniques. CA Cancer J Clin 2007;57:206-24.

17. Haralick R, Shanmugam K. Textural features for image classification. IEEE Trans Syst Man Cybern 1973;SMC-3:610-21.

18. Galloway M. Texture classification using gray level run length. Comput Graph Image Process 1975;4:172-9.

19. Thibault G, Angulo J, Meyer F. Advanced statistical matrices for texture characterization: Application to cell classification. IEEE Trans Biomed Eng 2014;61:630-7.

20. Amadasun M, King R. Textural features corresponding to textural properties. IEEE Trans Syst Man Cybern 1989;19:1264-74.

21. Mayerhoefer ME, Materka A, Langs G, Häggström I, Szczypiński P, Gibbs P, et al. Introduction to radiomics. J Nucl Med 2020;61:488-95.

22. Chen YH, Wang TF, Chu SC, Lin CB, Wang LY, Lue KH, et al. Incorporating radiomic feature of pretreatment 18F-FDG PET improves survival stratification in patients with EGFR-mutated lung adenocarcinoma. PLoS One 2020;15:e0244502.

23. Lue KH, Chu SC, Wang LY, Chen YC, Li MH, Chang BS, et al. Tumor glycolytic heterogeneity improves detection of regional nodal metastasis in patients with lung adenocarcinoma. Ann Nucl Med 2022;36:256-66.

24. Laine A, Fan J. Texture classification by wavelet packet signatures. IEEE Trans Pattern Anal Mach Intell 1993;15:1186-91.

25. Zwanenburg A, Vallières M, Abdalah MA, Aerts HJ, Andrearczyk V, Apte A, et al. The image biomarker standardization initiative: Standardized quantitative radiomics for high-throughput image-based phenotyping. Radiology 2020;295:328-38.

26. van Griethuysen JJ, Fedorov A, Parmar C, Hosny A, Aucoin N, Narayan V, et al. Computational radiomics system to decode the radiographic phenotype. Cancer Res 2017;77:e104-7.

27. Nioche C, Orlhac F, Boughdad S, Reuzé S, Goya-Outi J, Robert C, et al. LIFEx: A freeware for radiomic feature calculation in multimodality imaging to accelerate advances in the characterization of tumor heterogeneity. Cancer Res 2018;78:4786-9.

28. Kang F, Mu W, Gong J, Wang S, Li G, Li G, et al. Integrating manual diagnosis into radiomics for reducing the false positive rate of (18) F-FDG PET/CT diagnosis in patients with suspected lung cancer. Eur J Nucl Med Mol Imaging 2019;46:2770-9.

29. Kirienko M, Cozzi L, Rossi A, Voulaz E, Antunovic L, Fogliata A, et al. Ability of FDG PET and CT radiomics features to differentiate between primary and metastatic lung lesions. Eur J Nucl Med Mol Imaging 2018;45:1649-60.

30. Hyun SH, Ahn MS, Koh YW, Lee SJ. A machine-learning approach using PET-based radiomics to predict the histological subtypes of lung cancer. Clin Nucl Med 2019;44:956-60.

31. Han Y, Ma Y, Wu Z, Zhang F, Zheng D, Liu X, et al. Histologic subtype classification of non-small cell lung cancer using PET/CT images. Eur J Nucl Med Mol Imaging 2021;48:350-60.

32. Chen YH, Chen YC, Lue KH, Chu SC, Chang BS, Wang LY, et al. Glucose metabolic heterogeneity correlates with pathological features and improves survival stratification of resectable lung adenocarcinoma. Ann Nucl Med 2023;37:139-50.

33. Shao X, Niu R, Shao X, Jiang Z, Wang Y. Value of (18)F-FDG PET/CT-based radiomics model to distinguish the growth patterns of early invasive lung adenocarcinoma manifesting as ground-glass opacity nodules. EJNMMI Res 2020;10:80.

34. Laros SS, Dieckens D, Blazis SP, van der Heide JA. Machine learning classification of mediastinal lymph node metastasis in NSCLC: A multicentre study in a Western European patient population. EJNMMI Phys 2022;9:66.

35. Qiao J, Zhang X, Du M, Wang P, Xin J. (18)F-FDG PET/CT radiomics nomogram for predicting occult lymph node metastasis of non-small cell lung cancer. Front Oncol 2022;12:974934.

36. Huang Y, Jiang X, Xu H, Zhang D, Liu LN, Xia YX, et al. Preoperative prediction of mediastinal lymph node metastasis in non-small cell lung cancer based on (18)F-FDG PET/CT radiomics. Clin Radiol 2023;78:8-17.

37. Ren C, Zhang F, Zhang J, Song S, Sun Y, Cheng J. Clinico-biological-radiomics (CBR) based machine learning for improving the diagnostic accuracy of FDG-PET false-positive lymph nodes in lung cancer. Eur J Med Res 2023;28:554.

38. Zheng Z, Wang J, Tan W, Zhang Y, Li J, Song R, et al. (18)F-FDG PET/CT radiomics predicts brain metastasis in I-IIIA resected non-small cell lung cancer. Eur J Radiol 2023;165:110933.

39. Lv Z, Fan J, Xu J, Wu F, Huang Q, Guo M, et al. Value of (18)F-FDG PET/CT for predicting EGFR mutations and positive ALK expression in patients with non-small cell lung cancer: A retrospective analysis of 849 Chinese patients. Eur J Nucl Med Mol Imaging 2018;45:735-50.

40. Zhang J, Zhao X, Zhao Y, Zhang J, Zhang Z, Wang J, et al. Value of pre-therapy (18)F-FDG PET/CT radiomics in predicting EGFR mutation status in patients with non-small cell lung cancer. Eur J Nucl Med Mol Imaging 2020;47:1137-46.

41. Ge X, Gao J, Niu R, Shi Y, Shao X, Wang Y, et al. New research progress on 18F-FDG PET/CT radiomics for EGFR mutation prediction in lung adenocarcinoma: A review. Front Oncol 2023;13:1242392.

42. Yang B, Ji HS, Zhou CS, Dong H, Ma L, Ge YQ, et al. (18)F-fluorodeoxyglucose positron emission tomography/computed tomography-based radiomic features for prediction of epidermal growth factor receptor mutation status and prognosis in patients with lung adenocarcinoma. Transl Lung Cancer Res 2020;9:563-74.

43. Agüloğlu N, Aksu A, Akyol M, Katgı N, Doksöz TÇ. Importance of pretreatment 18F-FDG PET/CT texture analysis in predicting EGFR and ALK mutation in patients with non-small cell lung cancer. Nuklearmedizin 2022;61:433-9.

44. Yang L, Xu P, Li M, Wang M, Peng M, Zhang Y, et al. PET/CT radiomic features: A potential biomarker for EGFR mutation status and survival outcome prediction in NSCLC patients treated with TKIs. Front Oncol 2022;12:894323.

45. Liu Q, Sun D, Li N, Kim J, Feng D, Huang G, et al. Predicting EGFR mutation subtypes in lung adenocarcinoma using (18)F-FDG PET/CT radiomic features. Transl Lung Cancer Res 2020;9:549-62.

46. Ruan M, Liu L, Wang L, Lei B, Sun X, Chang C, et al. Correlation between combining (18)F-FDG PET/CT metabolic parameters and other clinical features and ALK or ROS1 fusion in patients with non-small-cell lung cancer. Eur J Nucl Med Mol Imaging 2020;47:1183-97.

47. Zhou J, Zou S, Kuang D, Yan J, Zhao J, Zhu X. A novel approach using FDG-PET/CT-based radiomics to assess tumor immune phenotypes in patients with non-small cell lung cancer. Front Oncol 2021;11:769272.

48. Zhao X, Zhao Y, Zhang J, Zhang Z, Liu L, Zhao X. Predicting PD-L1 expression status in patients with non-small cell lung cancer using [(18)F] FDG PET/CT radiomics. EJNMMI Res 2023;13:4.

49. Evangelista L, Fiz F, Laudicella R, Bianconi F, Castello A, Guglielmo P, et al. PET radiomics and response to immunotherapy in lung cancer: A systematic review of the literature. Cancers (Basel) 2023;15:3258.

50. Li J, Ge S, Sang S, Hu C, Deng S. Evaluation of PD-L1 expression level in patients with non-small cell lung cancer by (18)F-FDG PET/CT radiomics and clinicopathological characteristics. Front Oncol 2021;11:789014.

51. Dissaux G, Visvikis D, Da-Ano R, Pradier O, Chajon E, Barillot I, et al. Pretreatment (18)F-FDG PET/CT radiomics predict local recurrence in patients treated with stereotactic body radiotherapy for early-stage non-small cell lung cancer: A multicentric study. J Nucl Med 2020;61:814-20.

52. Lovinfosse P, Janvary ZL, Coucke P, Jodogne S, Bernard C, Hatt M, et al. FDG PET/CT texture analysis for predicting the outcome of lung cancer treated by stereotactic body radiation therapy. Eur J Nucl Med Mol Imaging 2016;43:1453-60.

53. Takeda K, Takanami K, Shirata Y, Yamamoto T, Takahashi N, Ito K, et al. Clinical utility of texture analysis of 18F-FDG PET/CT in patients with stage I lung cancer treated with stereotactic body radiotherapy. J Radiat Res 2017;58:862-9.

54. Valentinuzzi D, Vrankar M, Boc N, Ahac V, Zupancic Z, Unk M, et al. 18F FDG PET immunotherapy radiomics signature (iRADIOMICS) predicts response of non-small-cell lung cancer patients treated with pembrolizumab. Radiol Oncol 2020;54:285-94.

55. Yang M, Li X, Cai C, Liu C, Ma M, Qu W, et al. (18)F FDG PET-CT radiomics signature to predict pathological complete response to neoadjuvant chemoimmunotherapy in non-small cell lung cancer: A multicenter study. Eur Radiol 2024;34:4352-63.

56. Libling WA, Korn R, Weiss GJ. Review of the use of radiomics to assess the risk of recurrence in early-stage non-small cell lung cancer. Transl Lung Cancer Res 2023;12:1575-89.

57. Ahn HK, Lee H, Kim SG, Hyun SH. Pre-treatment (18)F-FDG PET-based radiomics predict survival in resected non-small cell lung cancer. Clin Radiol 2019;74:467-73.

58. Chen YH, Lue KH, Chu SC, Chang BS, Lin CB. The combined tumor-nodal glycolytic entropy improves survival stratification in nonsmall cell lung cancer with locoregional disease. Nucl Med Commun 2023;44:100-7.

59. Yoo J, Lee J, Cheon M, Kim H, Choi YS, Pyo H, et al. Radiomics analysis of (18)F-FDG PET/CT for prognosis prediction in patients with stage III non-small cell lung cancer undergoing neoadjuvant chemoradiation therapy followed by surgery. Cancers (Basel) 2023;15:2012.

60. Zuo Y, Liu Q, Li N, Li P, Zhang J, Song S. Optimal (18)F-FDG PET/CT radiomics model development for predicting EGFR mutation status and prognosis in lung adenocarcinoma: A multicentric study. Front Oncol 2023;13:1173355.

61. Billè A, Okiror L, Skanjeti A, Errico L, Arena V, Penna D, et al. Evaluation of integrated positron emission tomography and computed tomography accuracy in detecting lymph node metastasis in patients with adenocarcinoma versus squamous cell carcinoma. Eur J Cardiothorac Surg 2013;43:574-9.

62. Pijl JP, Nienhuis PH, Kwee TC, Glaudemans AW, Slart RH, Gormsen LC. Limitations and pitfalls of FDG-PET/CT in infection and inflammation. Semin Nucl Med 2021;51:633-45.

63. Zhang Y, Sheng J, Kang S, Fang W, Yan Y, Hu Z, et al. Patients with exon 19 deletion were associated with longer progression-free survival compared to those with L858R mutation after first-line EGFR-TKIs for advanced non-small cell lung cancer: A meta-analysis. PLoS One 2014;9:e107161.

64. Yu M, Chen S, Hong W, Gu Y, Huang B, Lin Y, et al. Prognostic role of glycolysis for cancer outcome: Evidence from 86 studies. J Cancer Res Clin Oncol 2019;145:967-99.

65. Ko CC, Yeh LR, Kuo YT, Chen JH. Imaging biomarkers for evaluating tumor response: RECIST and beyond. Biomark Res 2021;9:52.

66. Forde PM, Spicer J, Lu S, Provencio M, Mitsudomi T, Awad MM, et al. Neoadjuvant nivolumab plus chemotherapy in resectable lung cancer. N Engl J Med 2022;386:1973-85.

67. Tang X, Wu F, Chen X, Ye S, Ding Z. Current status and prospect of PET-related imaging radiomics in lung cancer. Front Oncol 2023;13:1297674.

68. Shea M, Costa DB, Rangachari D. Management of advanced non-small cell lung cancers with known mutations or rearrangements: Latest evidence and treatment approaches. Ther Adv Respir Dis 2016;10:113-29.

69. Xiao Z, Cai H, Wang Y, Cui R, Huo L, Lee EY, et al. Deep learning for predicting epidermal growth factor receptor mutations of non-small cell lung cancer on PET/CT images. Quant Imaging Med Surg 2023;13:1286-99.

70. Tau N, Stundzia A, Yasufuku K, Hussey D, Metser U. Convolutional Neural Networks in Predicting Nodal and Distant Metastatic Potential of Newly Diagnosed Non-Small Cell Lung Cancer on FDG PET Images. AJR Am J Roentgenol 2020;215:192-7

71. Lue KH, Chen YH, Chu SC, Chang BS, Lin CB, Chen YC, et al. A comparison of 18 F-FDG PET-based radiomics and deep learning in predicting regional lymph node metastasis in patients with resectable lung adenocarcinoma: A cross-scanner and temporal validation study. Nucl Med Commun 2023;44:1094-105.

72. Afshar P, Mohammadi A, Tyrrell PN, Cheung P, Sigiuk A, Plataniotis KN, et al. Formula: See text: Deep learning-based radiomics for the time-to-event outcome prediction in lung cancer. Sci Rep 2020;10:12366.

73. Lue KH, Chen YH, Chu SC, Lin CB, Wang TF, Liu SH. Prognostic value of combining clinical factors, (18)F-FDG PET-based intensity, volumetric features, and deep learning predictor in patients with EGFR-mutated lung adenocarcinoma undergoing targeted therapies: A cross-scanner and temporal validation study. Ann Nucl Med 2024;38:647-58.

74. Nguyen HS, Ho DK, Nguyen NN, Tran HM, Tam KW, Le NQ. Predicting EGFR mutation status in non-small cell lung cancer using artificial intelligence: A systematic review and meta-analysis. Acad Radiol 2024;31:660-83.

75. van Velden FH, Kramer GM, Frings V, Nissen IA, Mulder ER, de Langen AJ, et al. Repeatability of radiomic features in non-small-cell lung cancer [(18)F]FDG-PET/CT studies: Impact of reconstruction and delineation. Mol Imaging Biol 2016;18:788-95.

76. Desseroit MC, Tixier F, Weber WA, Siegel BA, Cheze Le Rest C, Visvikis D, et al. Reliability of PET/CT shape and heterogeneity features in functional and morphologic components of non-small cell lung cancer tumors: A repeatability analysis in a prospective multicenter cohort. J Nucl Med 2017;58:406-11.

77. Traverso A, Wee L, Dekker A, Gillies R. Repeatability and reproducibility of radiomic features: A systematic review. Int J Radiat Oncol Biol Phys 2018;102:1143-58.

78. Konert T, Everitt S, La Fontaine MD, van de Kamer JB, MacManus MP, Vogel WV, et al. Robust, independent and relevant prognostic 18F-fluorodeoxyglucose positron emission tomography radiomics features in non-small cell lung cancer: Are there any? PLoS One 2020;15:e0228793.

79. Chen YH, Lue KH, Lin CB, Chen KC, Chan SC, Chu SC, et al. Genomic and glycolytic entropy are reliable radiogenomic heterogeneity biomarkers for non-small cell lung cancer. Int J Mol Sci 2023;24:3988.

80. Oliver JA, Budzevich M, Zhang GG, Dilling TJ, Latifi K, Moros EG. Variability of image features computed from conventional and respiratory-gated PET/CT images of lung cancer. Transl Oncol 2015;8:524-34.

81. Xu H, Lv W, Zhang H, Ma J, Zhao P, Lu L. Evaluation and optimization of radiomics features stability to respiratory motion in (18)F-FDG 3D PET imaging. Med Phys 2021;48:5165-78.

82. Chen YH, Kan KY, Liu SH, Lin HH, Lue KH. Impact of respiratory motion on (18)F-FDG PET radiomics stability: Clinical evaluation with a digital PET scanner. J Appl Clin Med Phys 2023;24:e14200.

83. Wu G, Jochems A, Refaee T, Ibrahim A, Yan C, Sanduleanu S, et al. Structural and functional radiomics for lung cancer. Eur J Nucl Med Mol Imaging 2021;48:3961-74.

84. Venugopal VK, Vaidhya K, Murugavel M, Chunduru A, Mahajan V, Vaidya S, et al. Unboxing AI – Radiological insights into a deep neural network for lung nodule characterization. Acad Radiol 2020;27:88-95.

85. van der Vos CS, Koopman D, Rijnsdorp S, Arends AJ, Boellaard R, van Dalen JA, et al. Quantification, improvement, and harmonization of small lesion detection with state-of-the-art PET. Eur J Nucl Med Mol Imaging 2017;44:4-16.

86. Wagatsuma K, Miwa K, Sakata M, Oda K, Ono H, Kameyama M, et al. Comparison between new-generation SiPM-based and conventional PMT-based TOF-PET/CT. Phys Med 2017;42:203-10.

87. Wallis D, Soussan M, Lacroix M, Akl P, Duboucher C, Buvat I. An [18F] FDG-PET/CT deep learning method for fully automated detection of pathological mediastinal lymph nodes in lung cancer patients. Eur J Nucl Med Mol Imaging 2022;49:881-8.